An Investigation of Mechanical Properties of DNA Origami Nanostructures

HONORS THESIS

Submitted to

The Engineering Honors Committee

119 Hitchcock Hall

College of Engineering

The Ohio State University

Columbus, Ohio 43210

by

Daniel Turowski

5/18/2012

Abstract

Structural DNA nanotechnology is a rapidly growing field with a wide array of potential applications, such as solving basic problems in structural biology and biophysics, designing nanoscale engineering tools, enabling targeted drug delivery, and more broadly, creating self-assembling biological nanomachines and nanomaterials. Scaffolded DNA origami is a recently developed method of designing 3D nanoscale structures from DNA. With this approach, structures on the order of 100 nm can be designed with CAD-like software and self-assembled in solution. Previous research has proven the ability to create novel nanoscale structures via DNA origami, but there are several barriers to more widespread application of the technology to new areas. In order to build a structure (like a gear) or more complicated devices for specific applications, the mechanical properties of the construction material must be known. The theoretical method to model nanoscale mechanics treats DNA double helices as solid cylinders that are rigidly attached for their entire length. This research assesses this assumption, attempting to quantify how well the theoretical model predicts experimental mechanics. To examine the effect of cross section on persistence length, filaments with three cross sections (6-, 12-, and 18-helices) were designed, fabricated, and analyzed. The mean persistence length of the 6- and 18-helix filaments was 1,345 nm and 7,660 nm as compared to the theoretical values of 2,700 nm and 23,400 nm, respectively. The results of the 12-helix filaments were inconclusive. The experimental persistence length was found to lie near the middle of the range from the assumption that none of the helices were rigidly attached at any point (low end) to the assumption that the helices are all rigidly attached for the entire length (high end).

Acknowledgements

I would like to thank Professor Carlos Castro for his guidance and the opportunity to pursue undergraduate research. I would also like to thank the research team at the Nanoengineering and Biodesign Lab, particularly Alex Marras, Mike Hudoba, and Emily Briggs, for their knowledge and guidance.

I would also like to thank Ashok Krishnamurthy and Siddhartha Samsi from the Ohio Supercomputing Center for their assistance with the image processing efforts.

Table of Contents

List of Figures

List of Tables

1. Introduction

1.1 Background

DNA is one of the fundamental building blocks of not only our own bodies, but also all other living organisms. The most familiar form is the double-stranded helix, which consists of two backbones bonded by nucleobase pairs following Watson and Crick base pairing: adenine bonds with thymine, and cytosine bonds with guanine. Individual strands of DNA, shown below in Figure 1, have poor mechanical properties and are not a good building material. By manipulating this nucleobase pairing, or simply base pairing, DNA origami turns DNA into a viable building material.

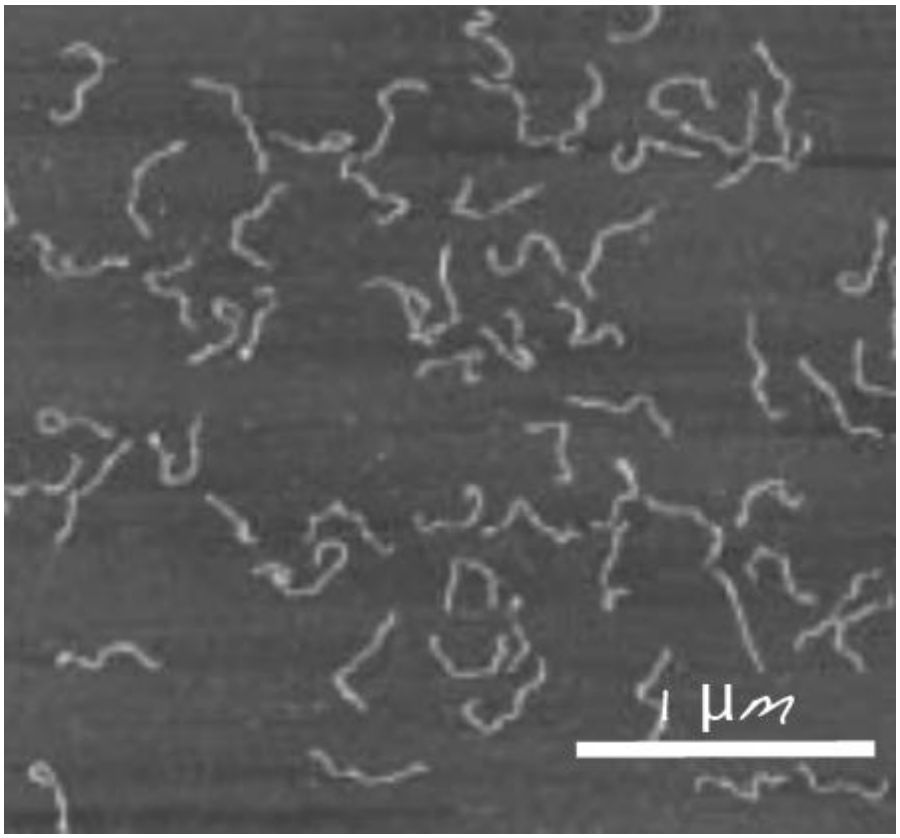

Figure 1: Atomic Force Microscopy (AFM) image of DNA strands (Pastre et al. 2003).

DNA origami is a method that utilizes DNA base pairing to create nanoscale structures that self-assemble in solution. As shown in Figure 2 below, the molecular components for assembly include a long, continuous "scaffold" strand (7000-8000 bases in length) and many much shorter "staple" strands (30-50 bases in length). The staples are designed to bond to the scaffold in a controlled manner in order to fold the scaffold strand into the desired 3D structure. Ultimately, these structures are comprised of bundles of double-stranded DNA arranged into the desired geometry.

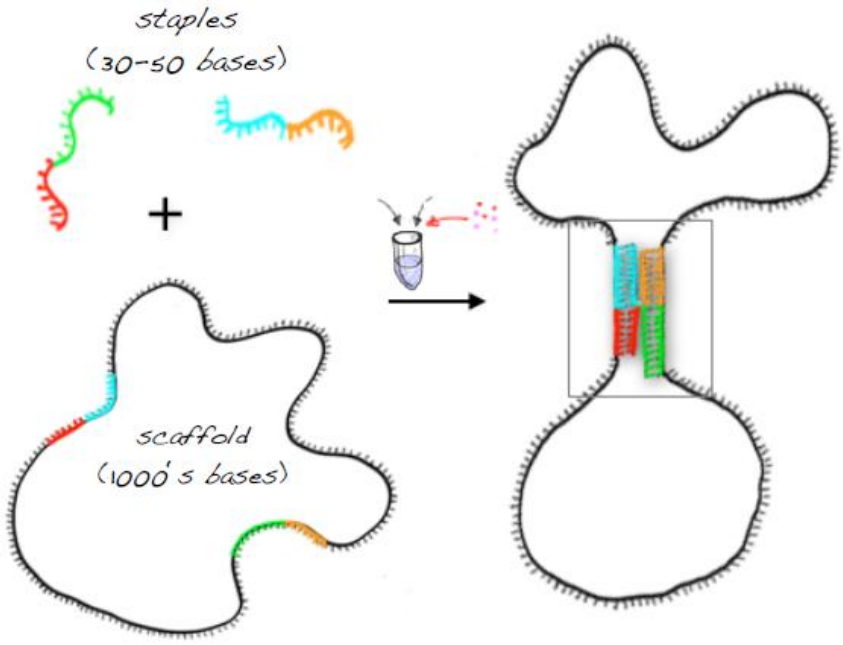

Figure 2: The bonding of shorter "staple" strands to longer, continuous "scaffold" strands can be manipulated to fold and create structures (Castro 2011).

The simple idea posed in Figure 2 is extended by a suite of CAD-like DNA origami design software (CaDNAno and CanDo) that facilitate the design of new structures. Figure 3 demonstrates how varying geometry is actually designed.

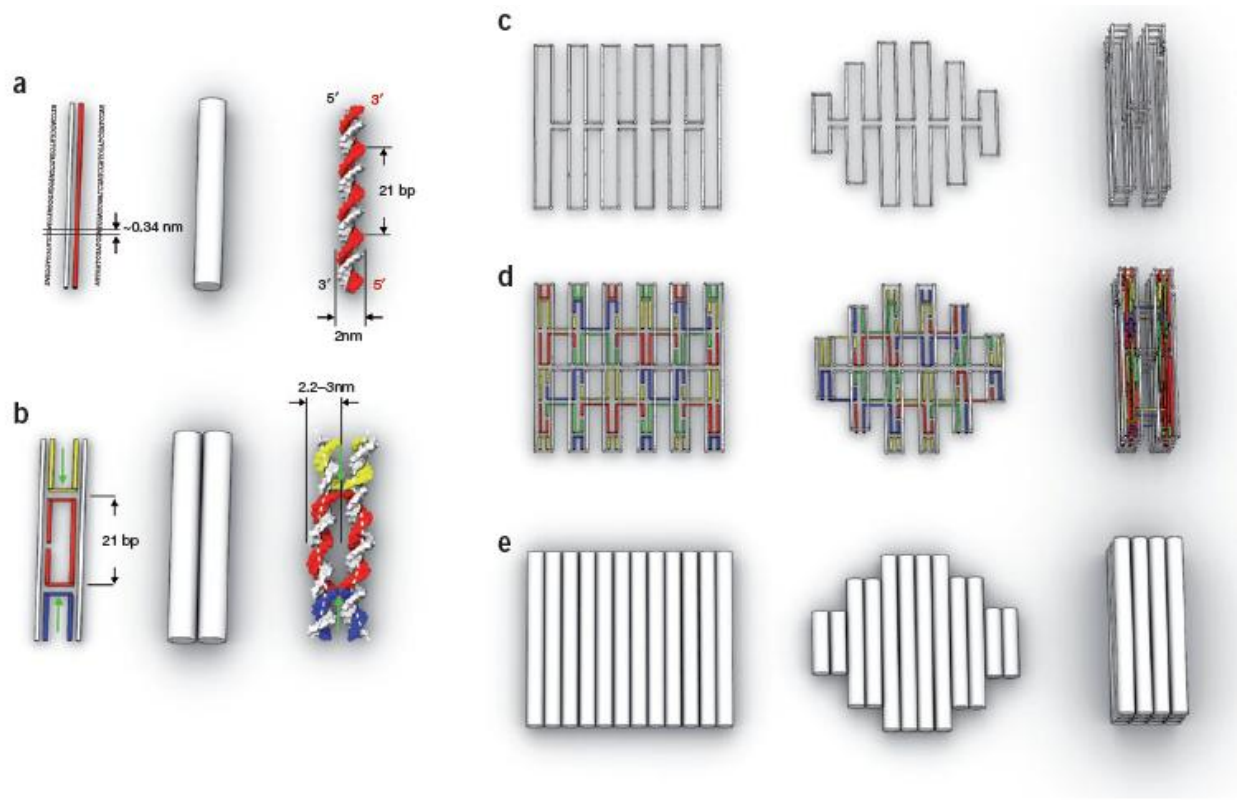

Figure 3: (a) DNA double helices are represented schematically as either two adjacent lines (left) or solid cylinders (middle). A detailed rendering of a double stranded helix is also shown (right). (b) Individual helices may be connected by crossovers (green arrows) of either the scaffold or staple strand. (c) Examples of single- and multilayer scaffold routing. (d) Examples of completed designs with colored staples bonded to the scaffold. (e) Structures represented by cylinders. (Castro 2011)

A variety of novel nanoscale geometries have been created to date, as seen in Figure 4. One application being researched at the Nanoengineering and Biodesign Lab focuses on designing and creating nanoscale force probes to measure the cellular traction forces of neutrophils (white blood cells) and fibroblasts. Another project focuses on creating nanoscale calipers for use as a nanoengineering tool. Another goal is to be able to create functional nanomaterials and nanostructures with adjustable mechanical properties. However, in order to effectively apply the existing knowledge of DNA origami to develop functional devices like those previously mentioned, a firm understanding of the mechanical properties of these structures is needed.

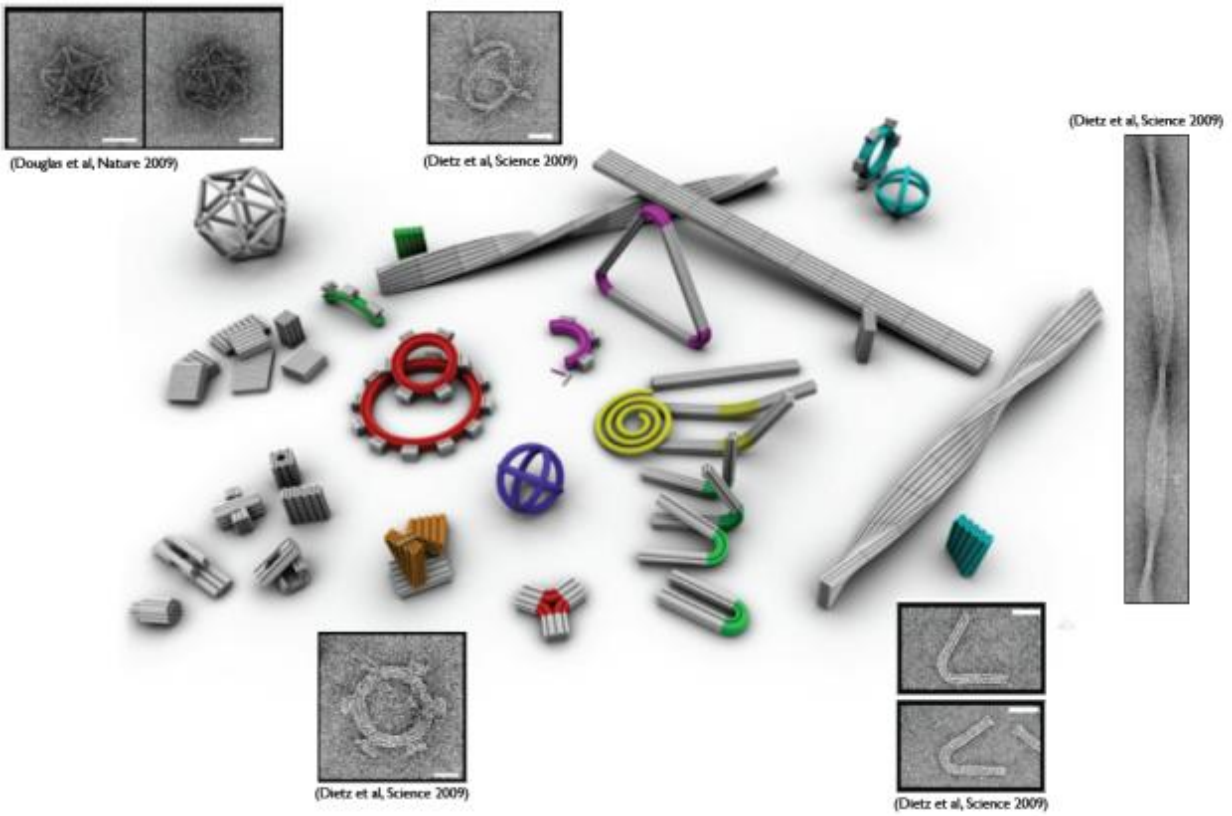

Figure 4: A collection of novel 3D geometry created via DNA origami (Castro 2011).

Just as with a macroscale gear, it is important to understand the mechanics when designing a nanoscale gear, such as that in Figure 5 below. Whether the gear is 100 mm or 100 nm in diameter, it is necessary to know how the gear will behave when subjected to bending or torsion, what the dynamics will be like, and so forth. These mechanics are not well understood at the nanoscale. Developing an understanding of the mechanics of DNA origami structures will enable effective and efficient design of devices for mechanical functions, in particular when creating larger assemblies from several DNA origami parts.

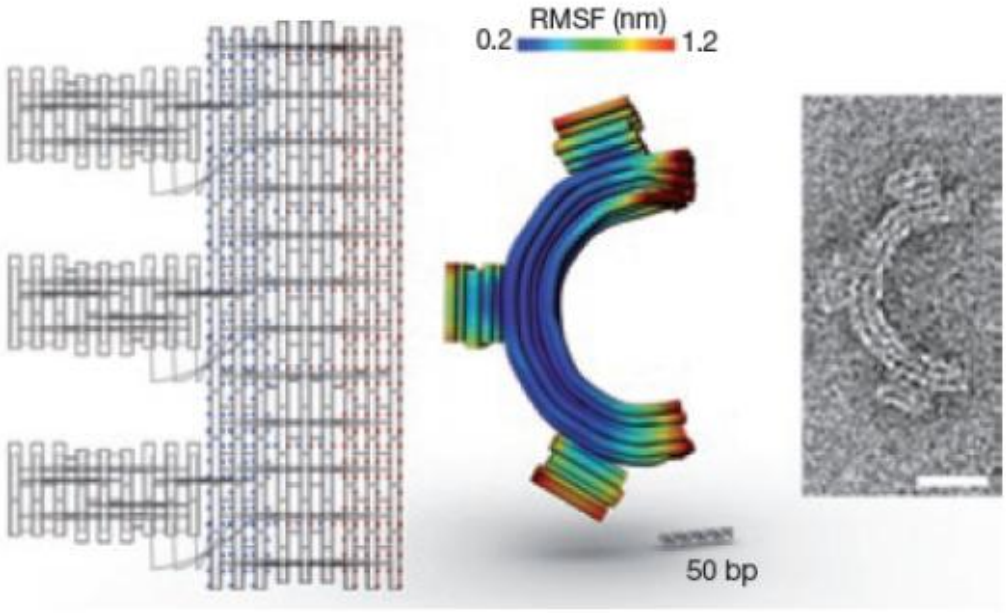

Figure 5: (left to right) A CAD design for the gear section depicted in the 3D model. Actual electron microscope image of the structure. (Castro 2011).

1.2 Focus of Thesis

Currently, DNA origami structures are modeled mechanically as a series of solid cylinders attached rigidly over their entire length. This assumption is known to be false, since helices are connected to each other typically only once every 21 bases.

The primary focus of this research project is to understand the mechanics of these nanoscale structures. Specifically, this research aims to assess the rigid coupling assumptions and quantify their accuracy. This was evaluated by looking at the effect of cross section on the stiffness of a DNA nanofilament. As additional DNA helices are added to a filament, the moment area of inertia is increased, resulting in a stiffer filament that deflects less. At the nanoscale, persistence length (l_p) is analogous to bending stiffness:

(1) $$l_p = \frac{E_{DNA} I_{DNA}}{k_B T} = \frac{B_s}{k_B T}$$

Persistence length is the measure of the flexibility of a polymer. It is a way of measuring the point at which a polymer can be treated statistically instead of elastically. In effect, if a polymer is much longer than its persistence length, it will bend and deflect readily. Conversely, if a polymer is much shorter than its persistence length, it will be very stiff and deflect very little. To predict the persistence length of a DNA origami filament, Equation 1 is manipulated as detailed below.

Double stranded DNA's diameter within a DNA origami structure is known to be approximately 2.5 nm. From this, the moment area of inertia can be approximated:

(2) $$I_{DNA} = \frac{\pi D^4}{64} = \frac{\pi(2.5\times10^{-9}\ \mathrm{m})^4}{64} = 1.92 \times 10^{-36}\ \mathrm{m}^4$$

For individual helices of double-stranded DNA, the persistence length has been estimated previously at 50 nm, which can be related to the elastic modulus:

(3) $$l_p = 5.0 \times 10^{-8}\ \mathrm{m} = \frac{E_{DNA} I_{DNA}}{k_B T}$$

The product of Boltzman's Constant k_B and temperature T is commonly valued at $k_B T = 4.1 \times 10^{-21}\mathrm{J\ per\ molecule} = 4.1\ \mathrm{pN \cdot nm}$. Using these values and the moment area of inertia calculated previously, the elastic modulus can be calculated:

(4) $$E_{DNA} = \frac{l_p k_B T}{I_{DNA}} = \frac{(5.0\times10^{-8}\ \mathrm{m})(4.1\ \mathrm{pN\cdot nm})}{1.92\times10^{-36}\ \mathrm{m}^4} = 1.07 \times 10^8\ \frac{\mathrm{N}}{\mathrm{m}^2}$$

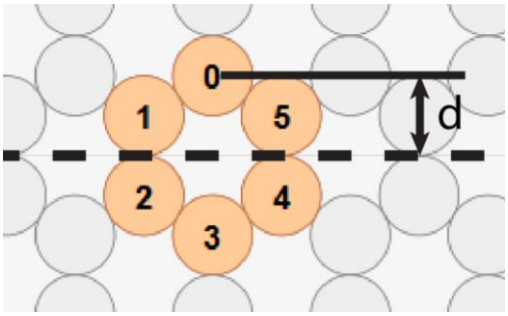

Figure 6: Parallel axis theorem performed on a 6 helix bundle about the x-axis.

The persistence length for an arbitrary DNA origami cross section consisting of double stranded helices can now be estimated by use of the parallel axis theorem, as shown in Figure 6 above for a 6 helix bundle:

(5) $$l_p^{6hb} = \frac{E_{DNA}[\Sigma(I_o + Ad^2)]}{k_B T} =$$

$$\frac{\left(1.07\times10^{8}\frac{\mathrm{N}}{\mathrm{m}^2}\right)\{2\cdot[(1.92\times10^{-36}\ \mathrm{m}^4)+(4.91\times10^{-18}\ \mathrm{m}^2)(2.5\ \mathrm{nm})^2]+4\cdot[(1.92\times10^{-36}\ \mathrm{m}^4)+(4.91\times10^{-18}\ \mathrm{m}^2)(1.25\ \mathrm{nm})^2]\}}{(4.1\ \mathrm{pN\cdot nm})} =$$

$$\frac{\left(1.07\times10^{8}\frac{\mathrm{N}}{\mathrm{m}^2}\right)\{2\cdot[3.3\times10^{-35}\ \mathrm{m}^4]+4\cdot[9.6\times10^{-36}\ \mathrm{m}^4]\}}{(4.1\ \mathrm{pN\cdot nm})} = 2{,}700\ \mathrm{nm}$$

Bending stiffness can then be calculated from the persistence length:

(6) $$B_s = E_{DNA} I_{DNA} = l_p k_B T = (2700\ \mathrm{nm})(4.1\ \mathrm{pN\cdot nm}) = 1.11\times10^{-26}\ \mathrm{N\cdot m^2}$$

This research project will compare the theoretical persistence length of 3 filaments using this method with experimentally determined values. Existing methods for measuring mechanical properties focus on persistence length, which is a convenient measure of bending stiffness for biological filaments. Persistence length can be calculated by tracking the shape fluctuations, specifically the tangent angle versus arc length trajectory, of a thermally fluctuating filament.

1.3 Significance of Research

This research quantifies the accuracy of theoretical models used to predict persistence length and bending stiffness. These theoretical models are based on assumptions which are known to be invalid; the stiffness of a crossover connecting two DNA helices is unknown, but the results may provide some insight into the mechanics of crossovers.

It is expected the bending stiffness of a polymer will be less than the value predicted because of misfolding and other assumptions made in the prediction. This research enables us to determine what cross section is needed to achieve a certain stiffness, based on the theoretical prediction. Eventually, the knowledge gained about nanoscale mechanics will make it easier to build up structures to larger scales than currently designed (up to 10's of microns, which is the size biological cells). Currently, most DNA origami structures are limited to a few microns in one dimension, but it is unknown how they will behave mechanically at larger sizes, such as 5 or more microns.

1.4 Overview of Thesis

Chapter 2 will discuss the procedure for designing the DNA origami filaments. It will then describe the process by which they were fabricated and imaged via Transmission Electron Microscopy. Chapter 3 contains the results and discusses the comparison of experimental and theoretical results. Chapter 4 concludes the thesis and discusses future work.

2. Procedure & Experimental Setup

The assumption of rigidly coupled helices was assessed by designing, fabricating, and imaging DNA origami filaments of varying cross section. The following sections detail the methods of designing DNA origami structures, the process of fabricating them, and imaging them. It also explains the method by which persistence length was experimentally measured.

2.1 Design

Filaments of three different cross sections, modeled in Figure 7 below, were designed such that they would have dissimilar persistence lengths. The approximate length and theoretical persistence length of each individual structure are summarized in Table 1 below.

Table 1: Comparison of cross sections tested.

Cross Section	Approximate Individual Bundle Length (nm)	Theoretical Persistence Length (nm)	Scaffold Strand Length (# of base pairs)
6 helix bundle	401.9	2,700	7308
12 helix bundle	201.0	12,600	7308
18 helix bundle	141.2	23,400	7704

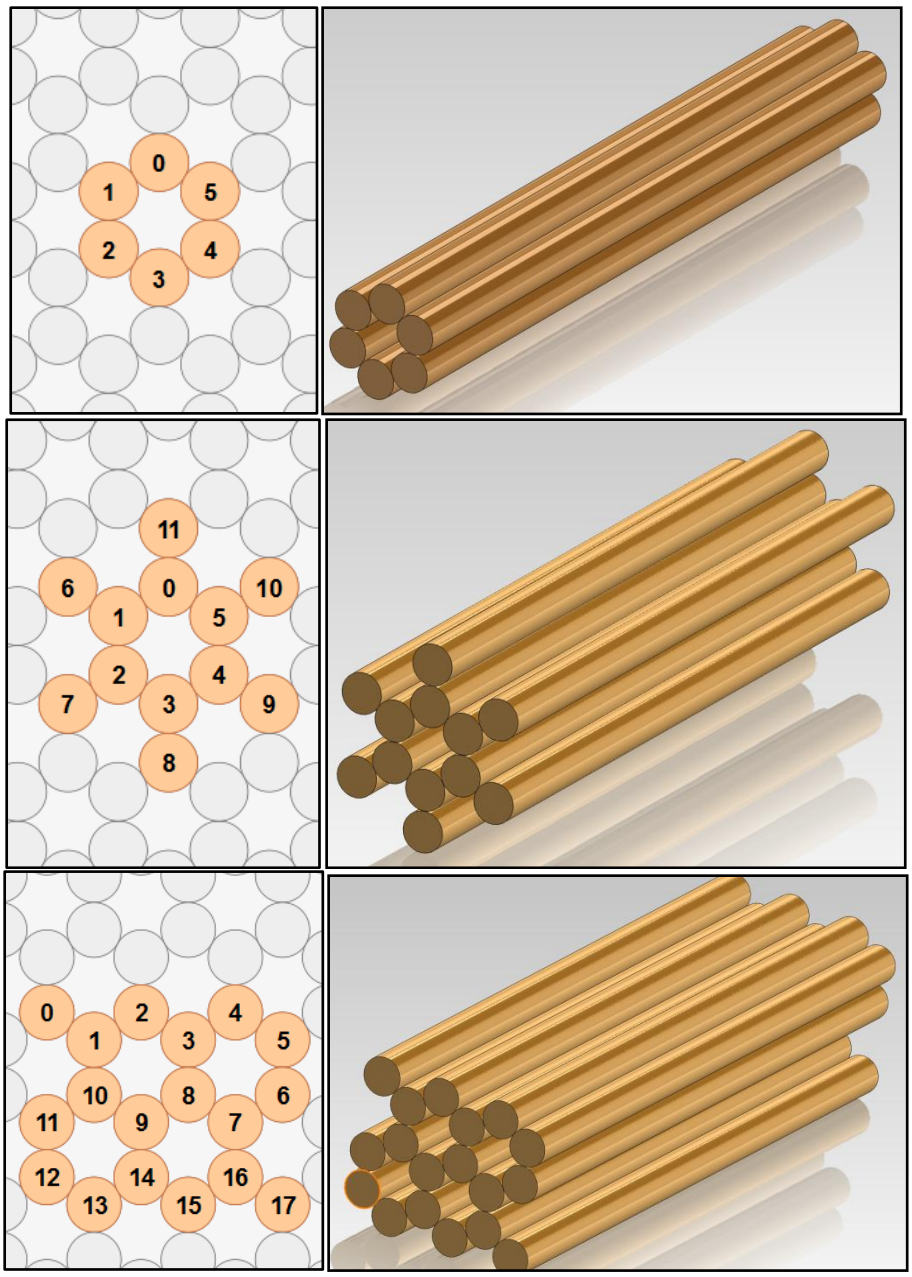

Figure 7: From top to bottom, the cross sections and solid models of the 6-, 12-, and 18-helix bundles.

As is seen in Table 1, the actual length of a 6 helix bundle would be approximately 401.9 nm, which is significantly less than its theoretical persistence length of 2,700 nm. As additional helices are used in the cross section, the individual bundle length decreases and the theoretical persistence length increases due to the increasing moment area of inertia.

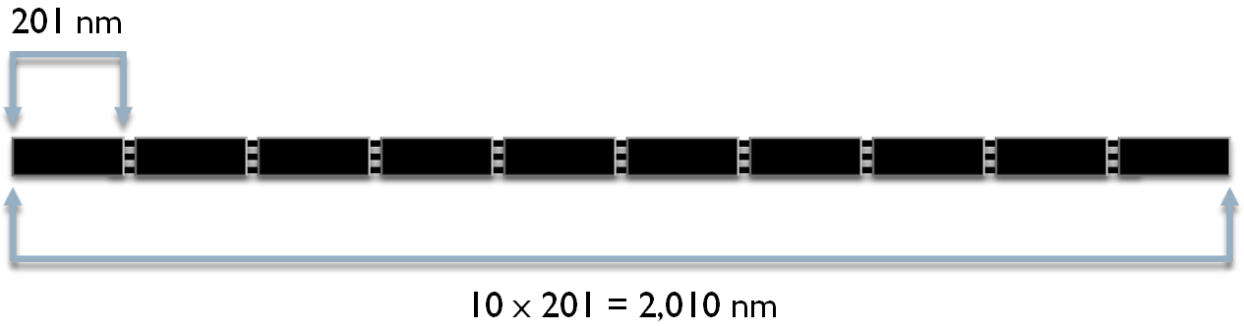

Figure 8: Diagram showing polymerization of individual 12 helix bundles into longer chains in order to experience measureable deflection.

Since the length of each of these three individual structures is well under their expected persistence lengths, little measureable deflection would be expected. In order to create filaments that are sufficiently long to experience significant deflection, the individual structures, or "bricks", were designed to be linked together to form long, polymerized chains, or filaments, as demonstrated in Figure 8 above. An example of the polymerization design between two "bricks" or monomers is shown in Figure 9 below. A detailed CaDNAno design of an individual structure is attached in Appendix A.

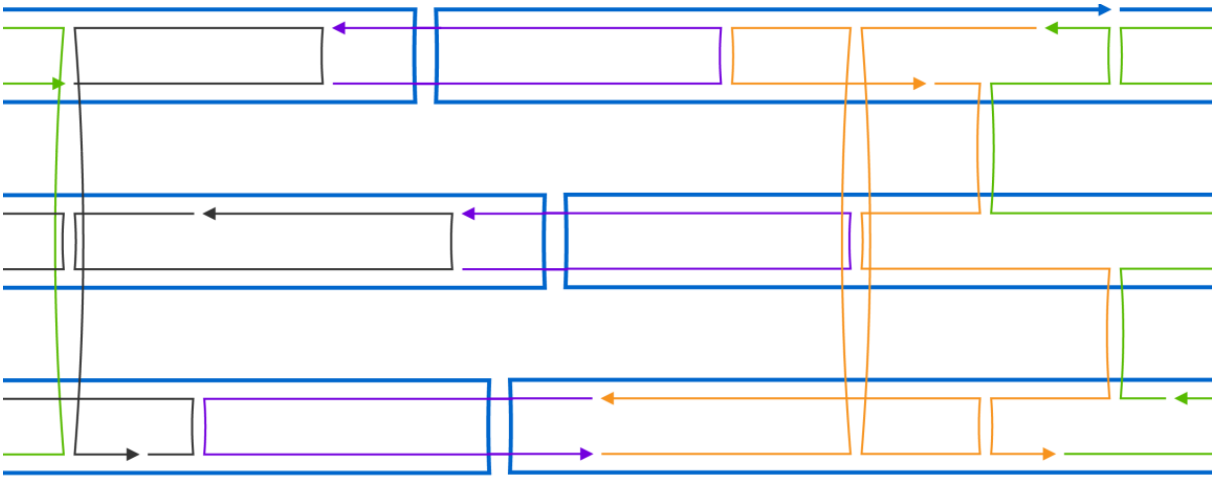

Figure 9: Example design of polymerization staples (purple) on the 6 helix bundle CaDNAno design.

2.2 Fabrication

The standard protocols used by the Nanoengineering and Biodesign Lab to create and image DNA origami structures are summarized below. These protocols are adapted from Douglas, SM., et al. (2007, 2009).

2.2.1 Folding Reactions

3D DNA origami objects are folded via molecular self-assembly reactions, which can be set up in a wide variety of ways. The current standard procedure at the Nanoengineering and Biodesign Lab involves mixing scaffold DNA, staple DNA, double distilled water, a buffer mastermix (to stabilize the pH), and magnesium ions in solution.

To facilitate the proper folding of the filaments, the staples are divided into groups known as pre-stocks. For example, the core staples form the bulk of the filament and are added first. The staples on the end of the filament are known as polymerization staples, as they join bundles together to form the long polymer chains that are the filaments. These staples are added last, as they are at the extremities of the structure. The staples that separate the core staples from the polymerization staples are grouped into “left end” and “right end” prestocks.

The pre-stocks used for each structure are identified in Table 2 below, including the color used to identify each group of staples on CaDNAno diagrams. A detailed CaDNAno design showing staple locations can be found in Appendix A.

Table 2: Summary of staple grouping (pre-stocks).

Pipette Order	Staple Group	CaDNAno Color	Function
#1	Core	Green	Largest bulk of the staples.
#2	Left End	Orange	Separate the core staples from the polymerization staples on the left end.
#3	Right End	Black	Separate the core staples from the polymerization staples on the right end.
#4	Polymerization	Purple	Connect the ends of two bundles.

Pre-stocks are combined into working stocks that contain all necessary staples to form the individual structures. Polymerization staples are omitted at this point in time to facilitate proper folding of the basic structure. Working stocks are then used to set up the folding reactions by combining them with the appropriate scaffold, water, magnesium screen consisting of various concentrations of $MgCl_2$, and a buffer (FOBXM). The components of a typical folding reaction are detailed in Table 3 below.

Table 3: Folding reaction for a working stock with 50 µl total volume and 20 nM effective scaffold concentration.

Components	Concentration	Volume (µl)
Scaffold	100 nM	10
Working Stock Staples	500 nM	20
FOBXM	50 mM TRIS, 10 mM EDTA	5
ddH_2O	N/A	10
$MgCl_2$ Mastermix	16 mM or 18 mM or 20 mM	5
Total		**50**

2.2.2 Thermal Ramp

After thoroughly mixing the solution, it is subjected to a thermal cycle that causes the scaffold and staple strands to bind together and fold the scaffold strand into the designed geometry. The folding reaction is heated up to melt all of the interactions between the nucelobases, and then it is cooled down slowly to control the binding, facilitating folding. A thermal ramp lasting approximately 2.5 days was utilized in this experiment.

2.2.3 Purification via Agarose Gel Electrophoresis

Once the thermal ramp is complete, the structures are folded and in solution with misfolded structures and unbounded staples. In order to separate well-folded structures from the other unwanted material, the solution is purified in an agarose gel stained with ethidium bromide (EtBr), which will make the structures visible under UV light. An agarose gel is shown in Figure 10 below, where the structures from the thermal ramp are dyed purple, placed in wells at one end, and immersed in a buffer solution. A voltage of 70V is applied across the gel; since DNA is negatively charged, it is drawn toward the positive (red) electrode at the other end.

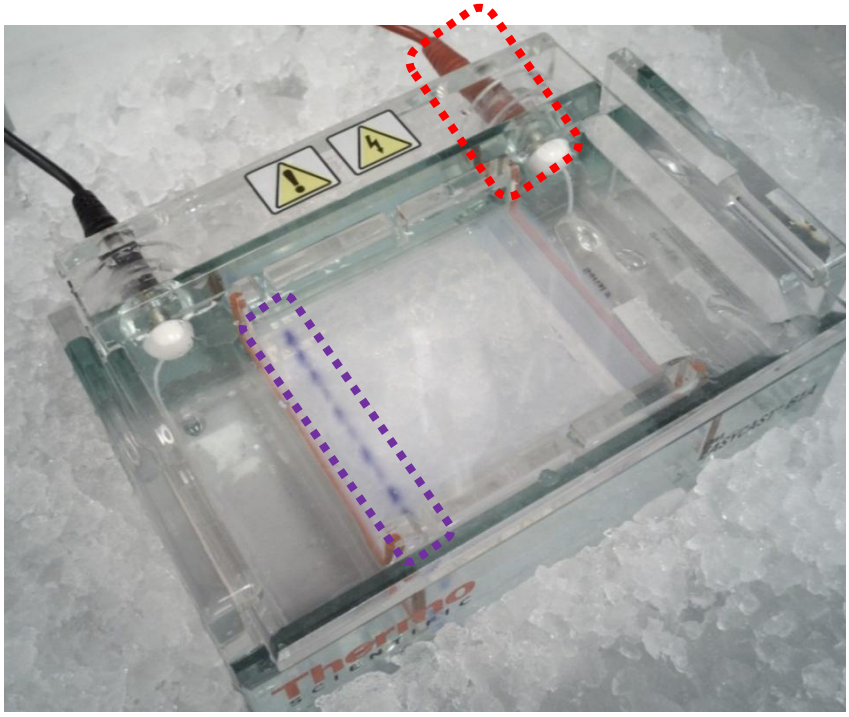

Figure 10: The agarose gel in an ice bath, subjected to a 70V current. Structures in the wells (purple) are negatively charged and drawn toward the positive (red) electrode.

The staple strands are much smaller than the folded structures, so they travel faster toward the positive pole, whereas misfolded structures are larger and will travel more slowly. Well-folded structures travel at similar speeds and are expected to be group relatively closely together. After 3 hours, the solution is segregated into distinct bands, seen in the UV image in Figure 11 below. The desired bands are cut out and filtered in a centrifuge in order to remove excess agarose, leaving only the well-folded structures in solution. A sample is prepared in order to look at the individual structures with the TEM. The remaining structures will be polymerized into filaments.

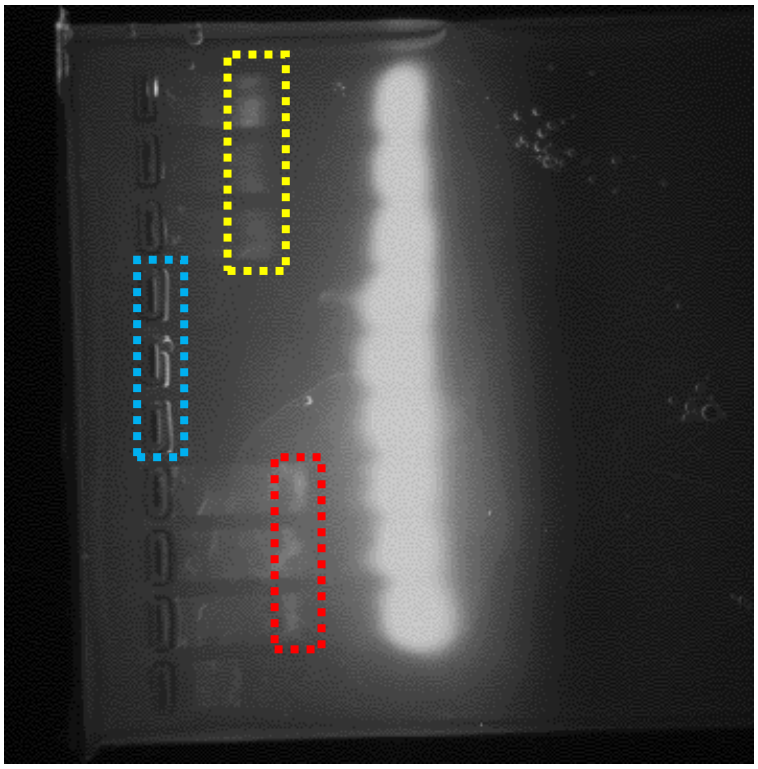

Figure 11: UV image of the agarose purification gel. The brightest spots are the high concentration of staple strands. The 6-helix (yellow) and 18-helix (red) bundles have distinct bands where well-folded structures are grouped. The 12-helix (blue) bundles are trapped at the starting point in the wells.

2.2.4 Polymerization

Once the individual structures have been purified, a secondary folding reaction is started with the individual "bricks" and excess polymerization staples. They are placed in solution in a ratio of 5:1 staples to bricks, which will be sufficiently low to avoid needing to re-purify the solution. They are then mixed and heated at 37^{o}C for 12 hours. The resulting solution will contain polymerized filaments, excess polymerization staples, and excess "bricks".

2.2.5 Negative-Staining for Transmission Electron Microscopy

Once the samples have been prepared, each is applied to a TEM grid. They are stained with a uranyl formate (UFo) solution to make them visible on the TEM. The samples are now ready for imaging.

2.3 Measurements

Once TEM images of the polymerized filaments were captured, they were analyzed to determine the persistence length. Persistence length was calculated by use of the tangent angle correlations:

$$\cos(\theta_s - \theta_0) = e^{-\frac{s}{2l_p}} \quad (7)$$

where

$\theta_0 = angle\ from\ horizontal\ at\ starting\ point$

$\theta_s = angle\ from\ horizontal\ at\ incremental\ point$

$s = arc\ length$

The calculations were performed by tracing a filament with a MATLAB script, which discretized it into finite segments via cubic splines, as shown in Figure 12 below. The persistence length for each segment was calculated, eventually calculating the average persistence length over the entire length of the filament.

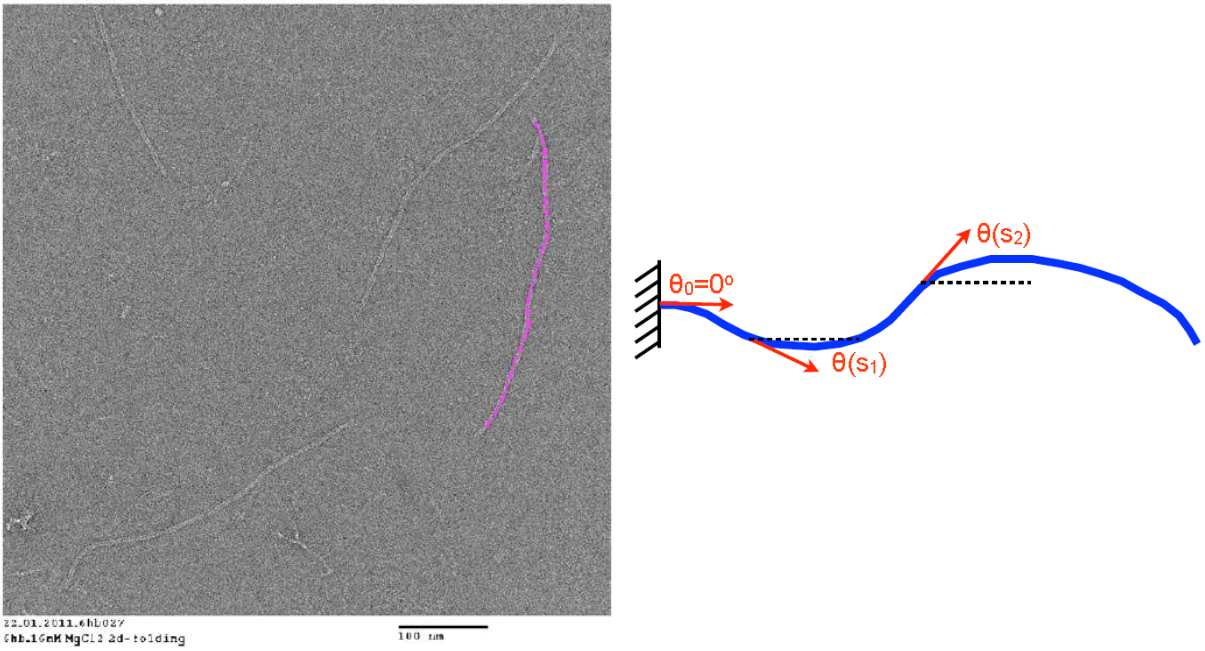

Figure 12: (left) A sample filament highlighted by the MATLAB script, which is (right) broken down into discrete sections to allow for the calculation of an average persistence length over the entire length (Dietz et al. 2011).

3. Results and Discussion

Sample images of the 3 individual structures are shown in Figures 13, 14, and 15. Images of the 6- and 18-helix polymerized filaments are contained below in Figures 18 and 19. The 12-helix structures were not successfully polymerized and no filaments are shown.

3.1 TEM Images

3.1.1 Individual Structures

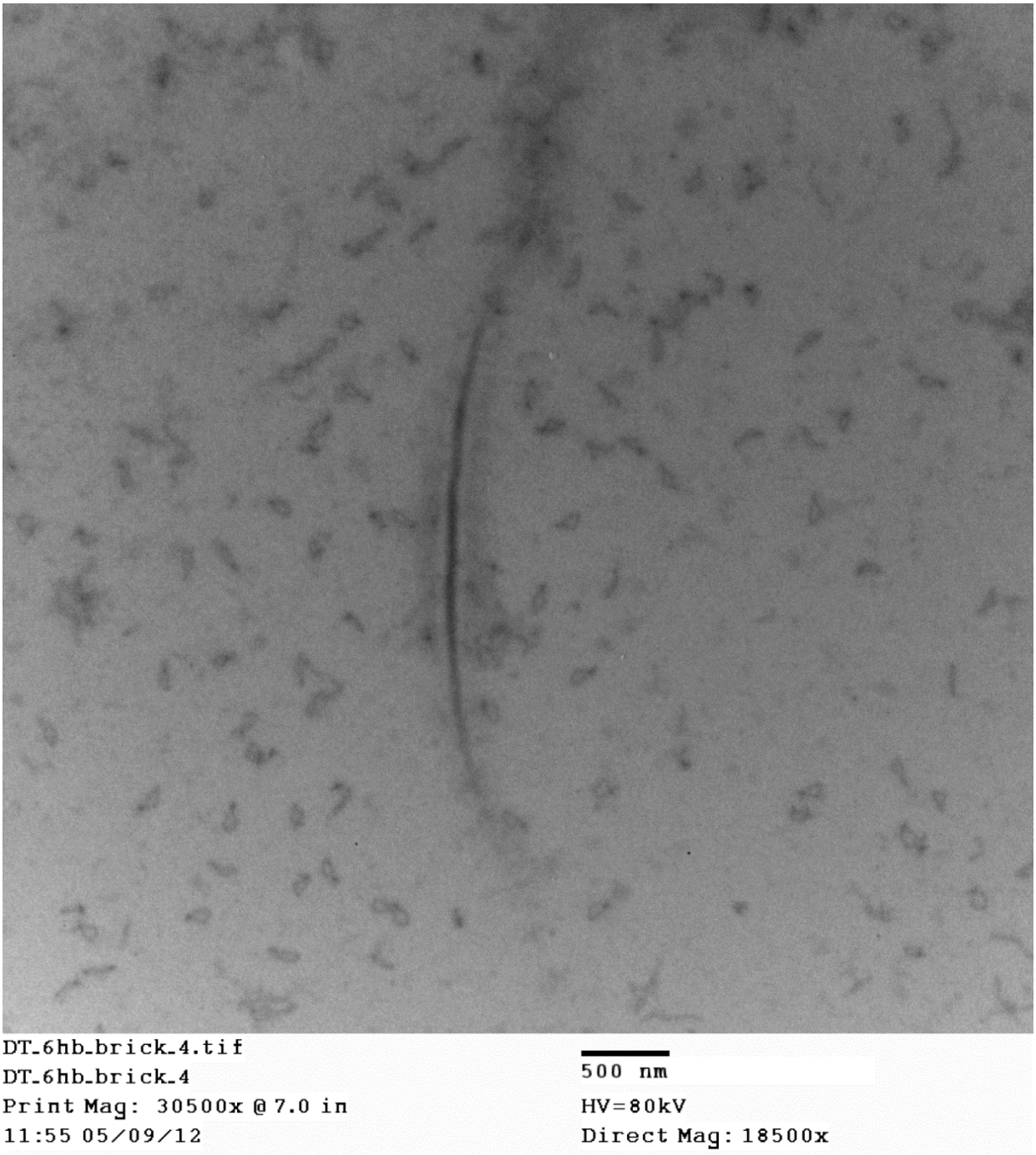

Figure 13: The individual bricks of the 6 helix bundle filaments at low magnification.

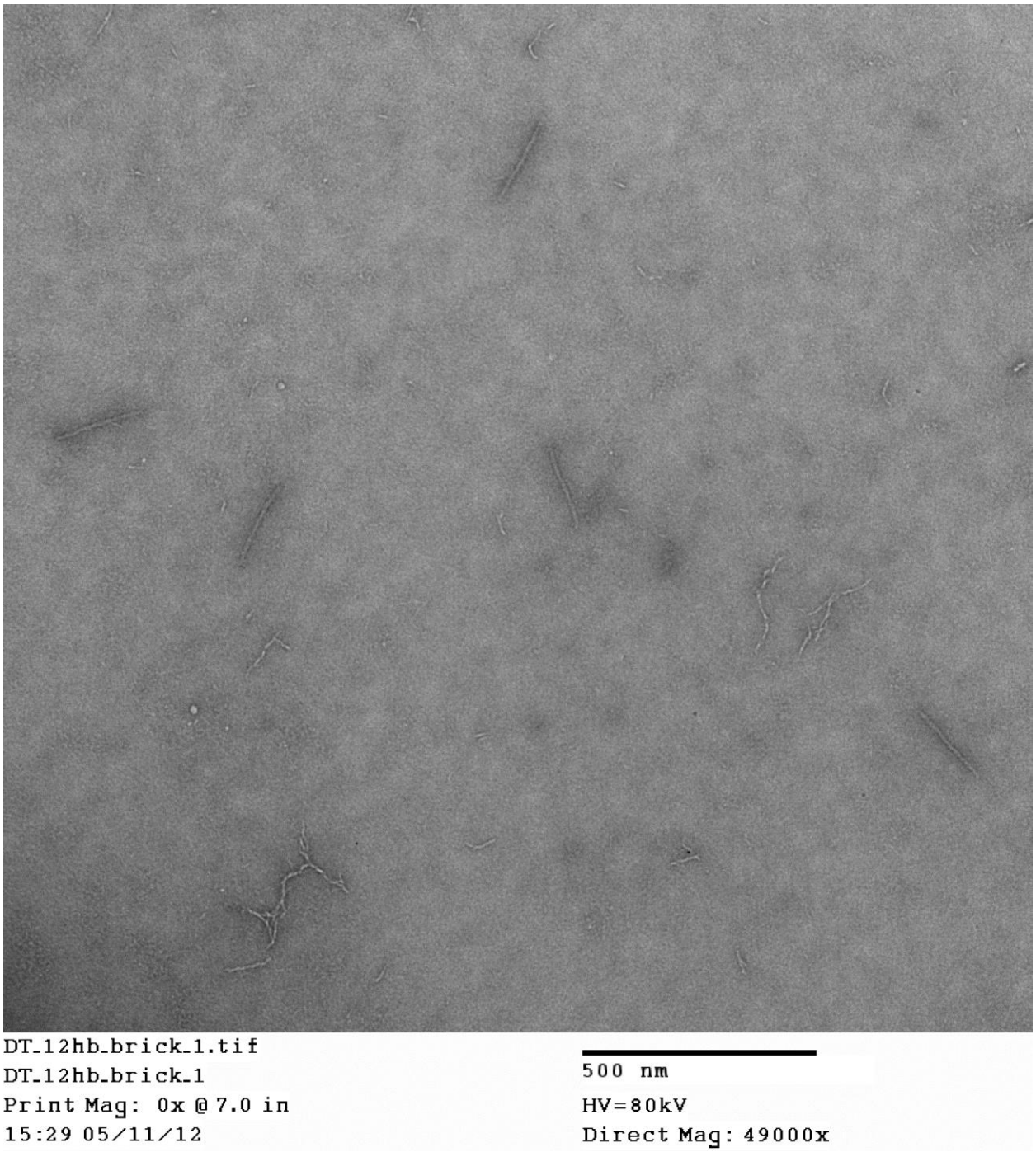

Figure 14: The individual bricks of the 12 helix bundle filaments.

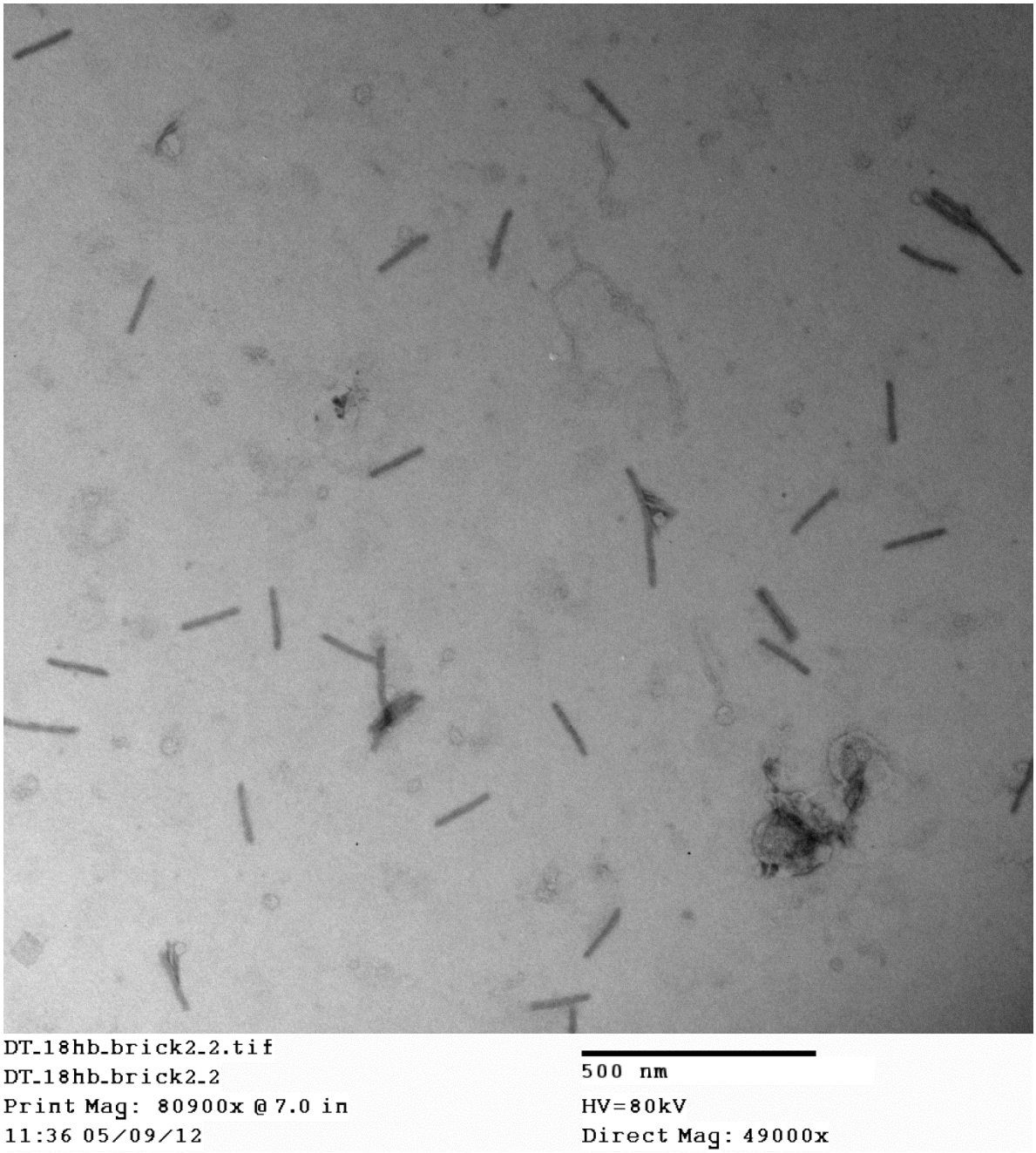

Figure 15: The individual bricks of the 18 helix bundle filaments.

There was a low yield of 12 helix bundles, which resulted in insufficient concentration of mers to polymerize them into filaments. It was suspected that the bundles were sticking to each other, as shown in Figure 16 below. This clumping prevented the bundles from entering

the purifying gel. To reduce the clumping effect, the structures were re-folded with only the core staples, eliminating the left and right end groups of staples. The goal was to reduce the propensity for the structures to stick to each other. The purifying gel image in Figure 17 shows that this was effective at improving the concentration of structures. However, insufficient time was available to polymerize and examine these structures for this experiment.

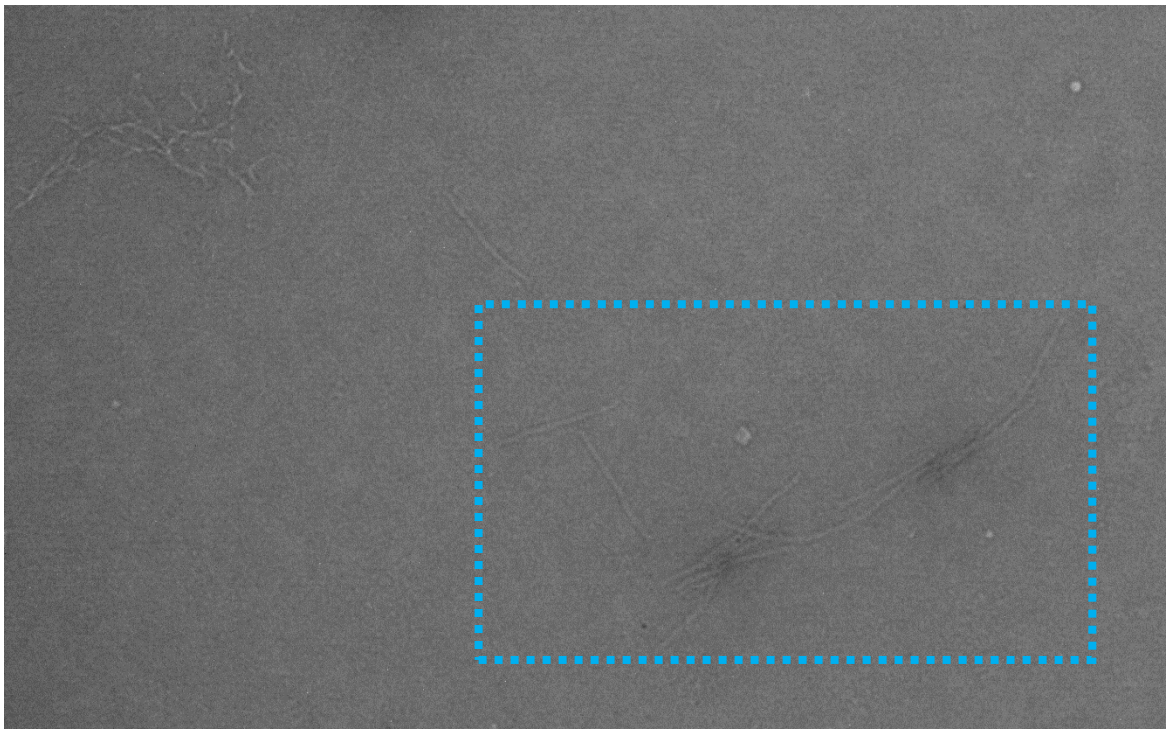

Figure 16: 12 helix bundles prior to purification showing how multiple structures stuck together, preventing them from entering the purifying gel and leading to a low yield of 12 helix bundles.

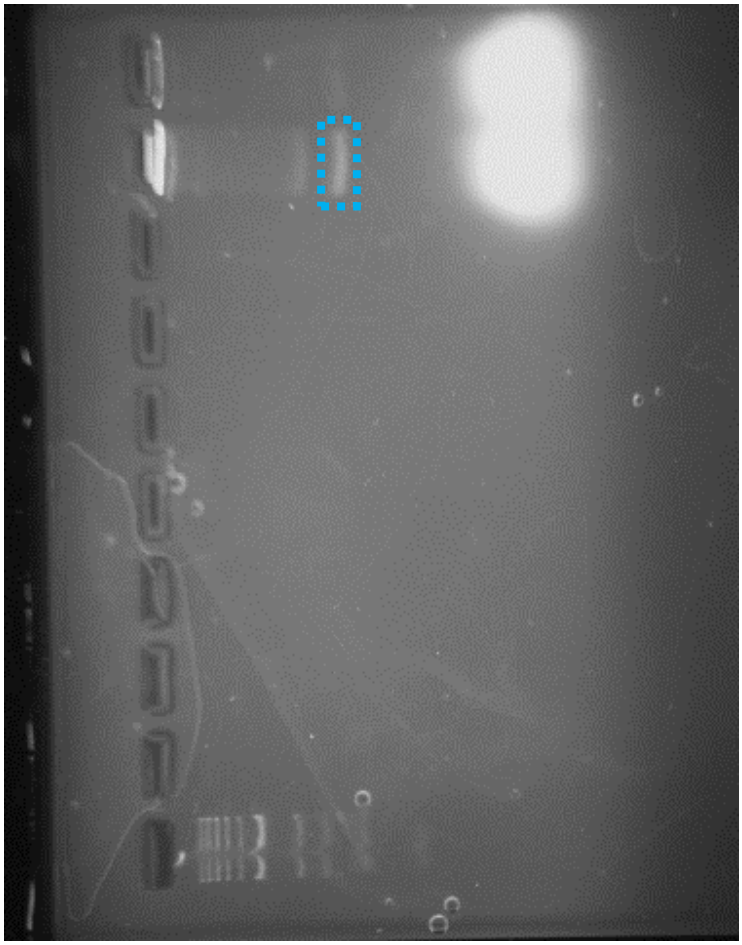

Figure 17: Image of purifying gel showing improved 12-helix bundle yield (blue).

3.1.2 Polymerized Filaments

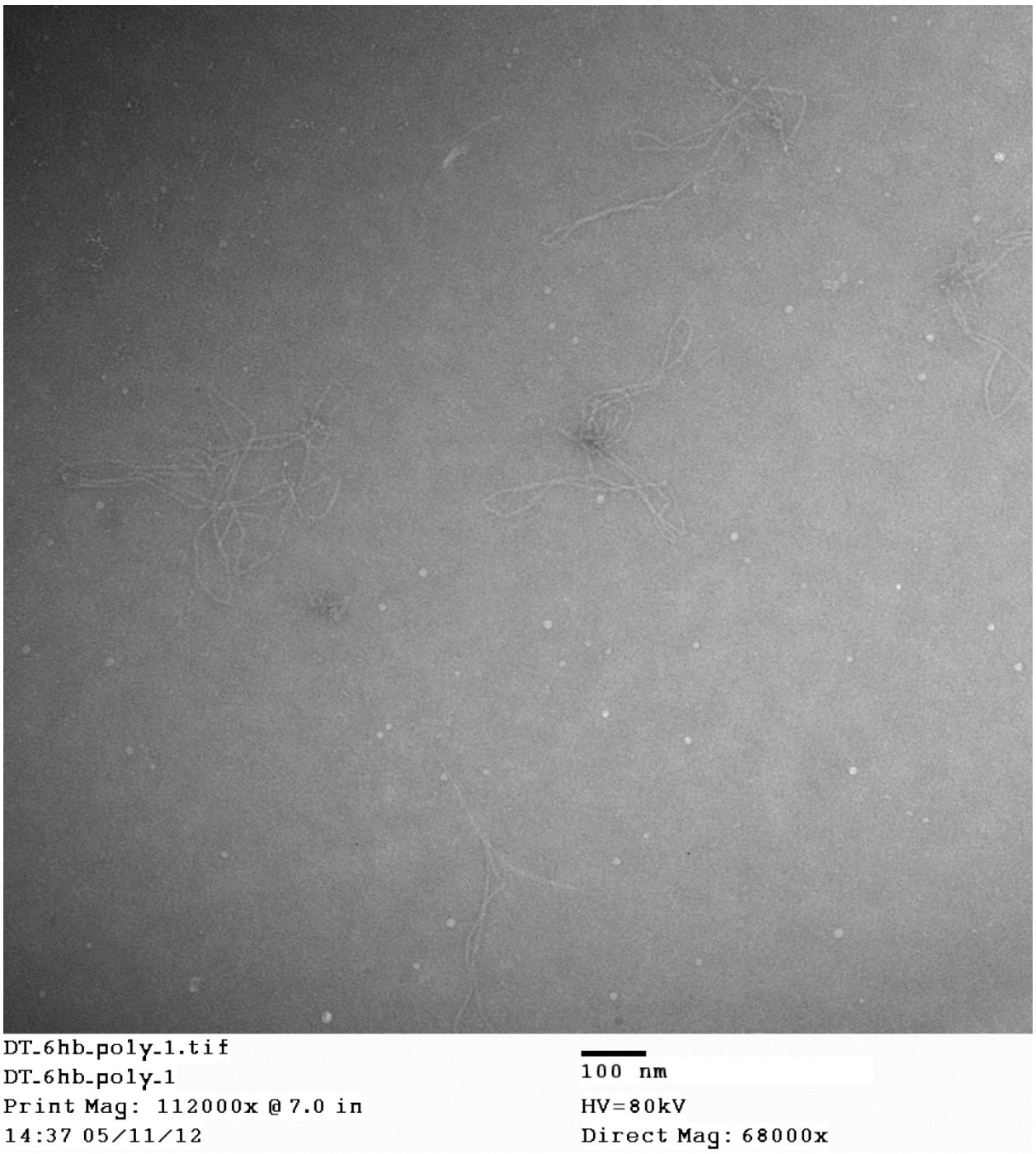

Figure 18: Polymerized 6 helix bundle filaments.

The 6 helix polymers were consistently tangled together and could not be individually measured. Because the individual structures appeared well-folded, better filaments could be constructed in the future by experimenting with the polymerization conditions.

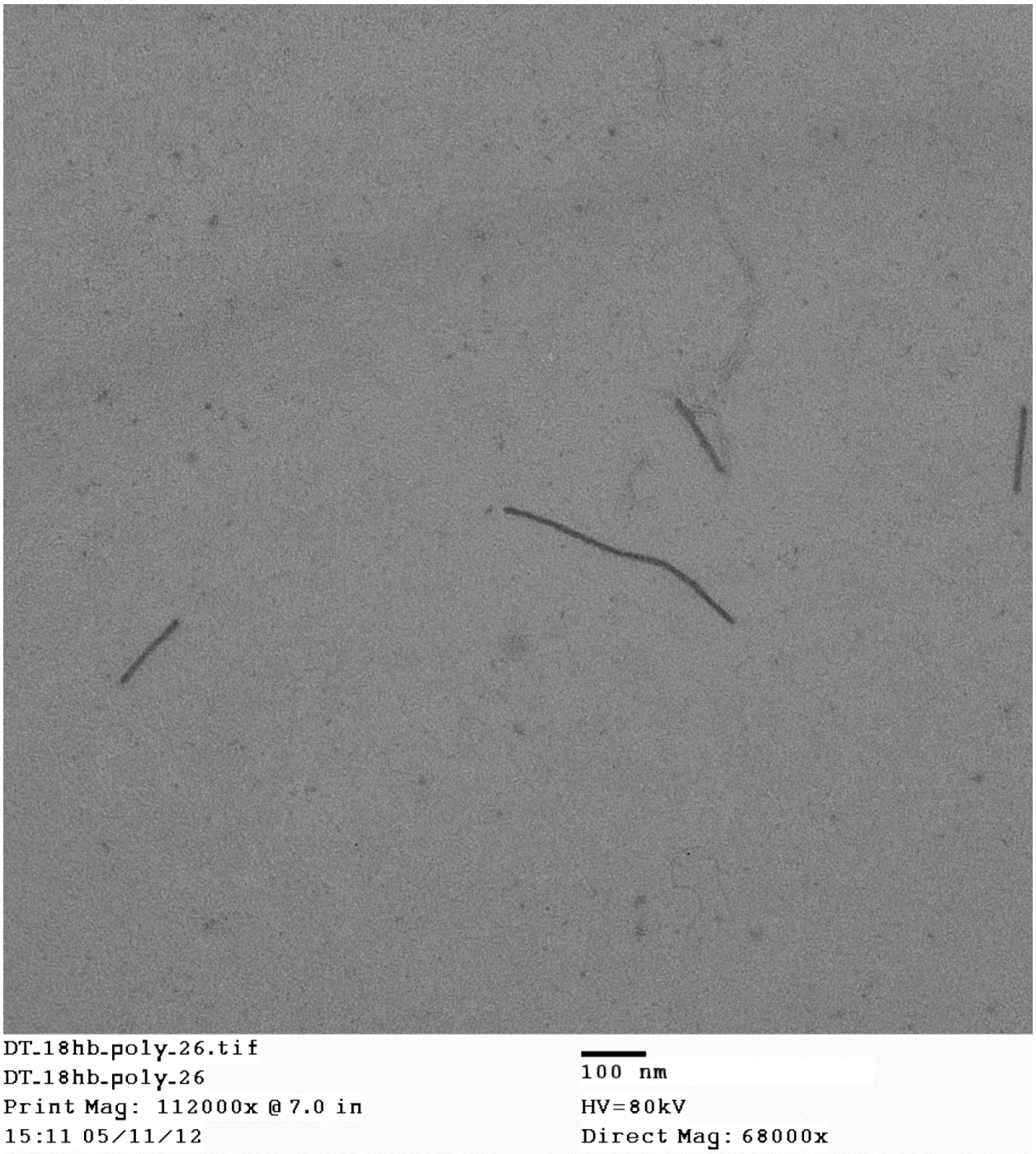

Figure 19: Polymerized 18 helix bundle filaments.

The longest 18 helix bundle polymers found had at most 5-6 monomers, with most filaments consisting of only 2 (dimers) or 3 (trimers). These were insufficiently long to exhibit enough deflection to measure the persistence length.

3.2 Persistence Length

The filaments observed were at most 4-5 monomers in length, which was a consequence of low concentration of individual monomers. In order to make reasonable measurements, polymers with around 10 or more monomers are needed; the experimental results obtained could not be analyzed. However, images of 6- and 18-helix bundles from previous experiments were available and therefore analyzed to find the persistence length of visible filaments. Histograms of the persistence length for the 6- and 18-helix cross sections can be seen in Figures 20 and 21 below. Table 4 summarizes the persistence length results and compares them with the theoretical values predicted.

Table 4: Summary of persistence length analysis.

Cross Section	# Samples	Standard Deviation (nm)	Persistence Length l_p (nm)			Percent Difference
			Median	Mean	Theoretical	
6 helix bundle	46	956	1,069	1,345	2,700	50.2%
12 helix bundle	N/A	N/A	N/A	N/A	12,600	N/A
18 helix bundle	32	15,013	5,438	7,660	23,400	67.3%

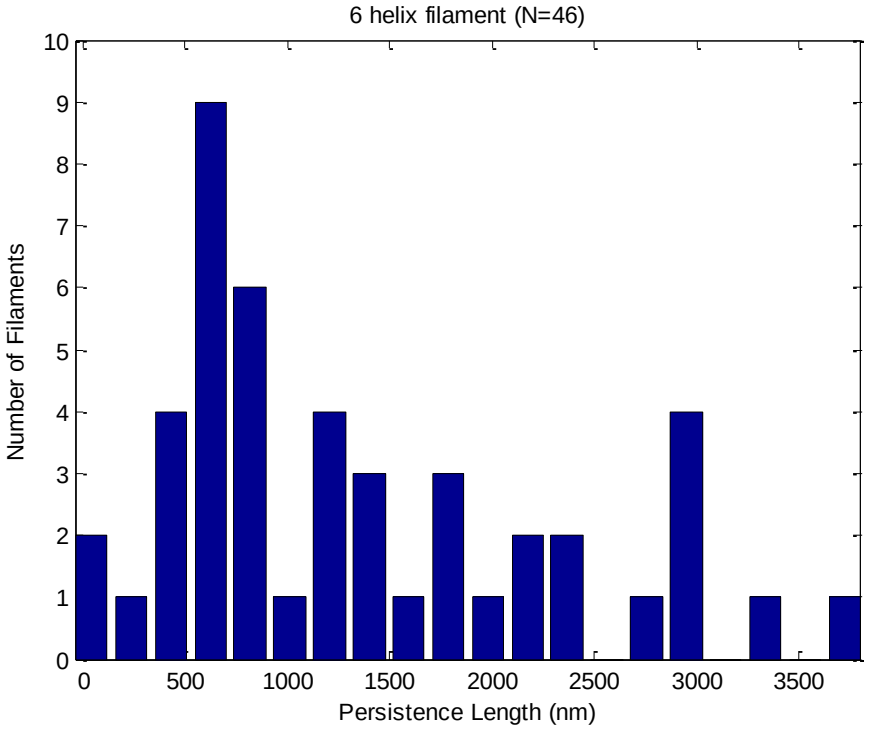

Figure 20: Statistical distribution of persistence length for the 6 helix bundle.

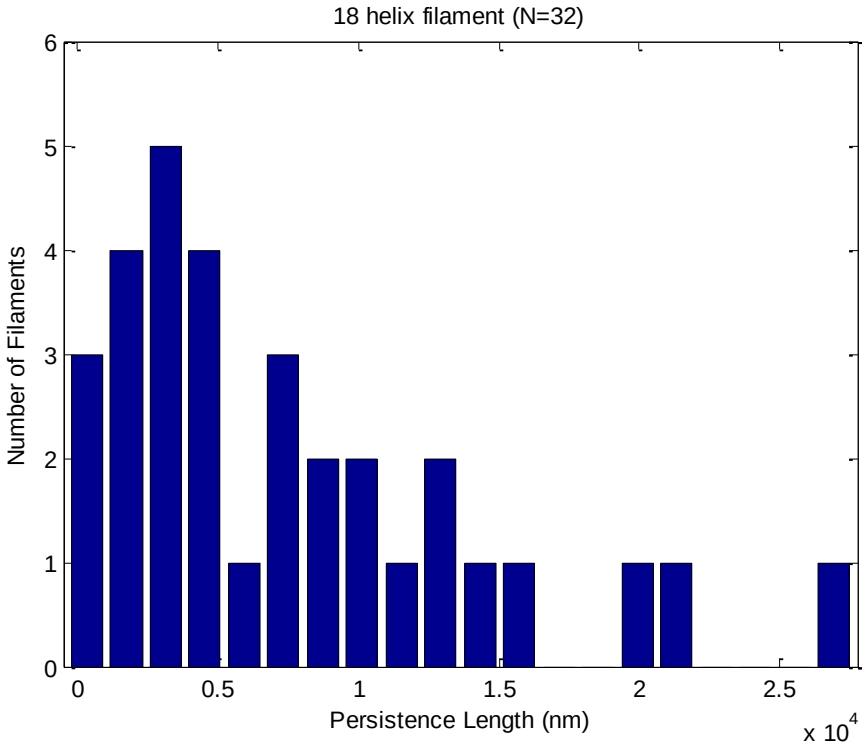

Figure 21: Statistical distribution of persistence length for the 18 helix bundle.

Although the persistence length was experimentally determined to be much less than the theoretical prediction, assuming the helices are rigidly attached for the entire length can be viewed as a high end of the range for persistence length. The low end of the range would be to assume the helices are not attached at all for the entire length. The persistence length in that case would be an integer multiple of the persistence length of an individual strand:

(8) $l_p = n l_p^0$

For a 6 helix bundle:

(9) $l_p = (6)(50\ \mathrm{nm}) = 300\ \mathrm{nm}$

This would suggest that the viable range of persistence lengths for a 6-helix filament would be from 300 nm – 2,700 nm. Similarly, the range for a 12-helix filament would be 600 nm – 12,600 nm, and the range for an 18-helix filament would be 900 nm – 23,400 nm.

4. Conclusion

The mean persistence length of the 6-helix filament was 1,345 nm with a standard deviation of 956 nm, compared to the theoretical value of 2,700 nm, which was a 50.2% difference. The mean persistence length of the 18-helix filament was 7,660 nm with a standard deviation of 15,013 nm, compared to the theoretical value of 23,400 nm, which was a 67.3% difference. The results of the 12-helix filaments were inconclusive.

The mean and median 6- and 18-helix filaments were all less than half of the theoretical value predicted. It can be seen that the resultant DNA origami structures have significantly lower persistence length than the theoretical values predicted by treating the DNA helices as rigidly attached solid cylinders. The other end of the range of possible persistence lengths would be to assume that the individual DNA helices are uncoupled for the entire length. In effect, the experimental persistence lengths were found to lie near the middle of this range from completely uncoupled to completely coupled. A larger sample size of 200 images per polymer design would be desirable to examine before making any further conclusions about the theoretical model.

4.1 Future Work

The current method of analyzing TEM images is a time-consuming process that may take 10 hours for a few hundred images. Through a collaboration with the Ohio Supercomputer Center, we have begun automating this process. One of the objectives is to generalize the image processing algorithms to be able to analyze images with more widely varying geometry.

An example of work to date can be seen in Figure 22 below, where nanocalipers are identified and the angle is measured.

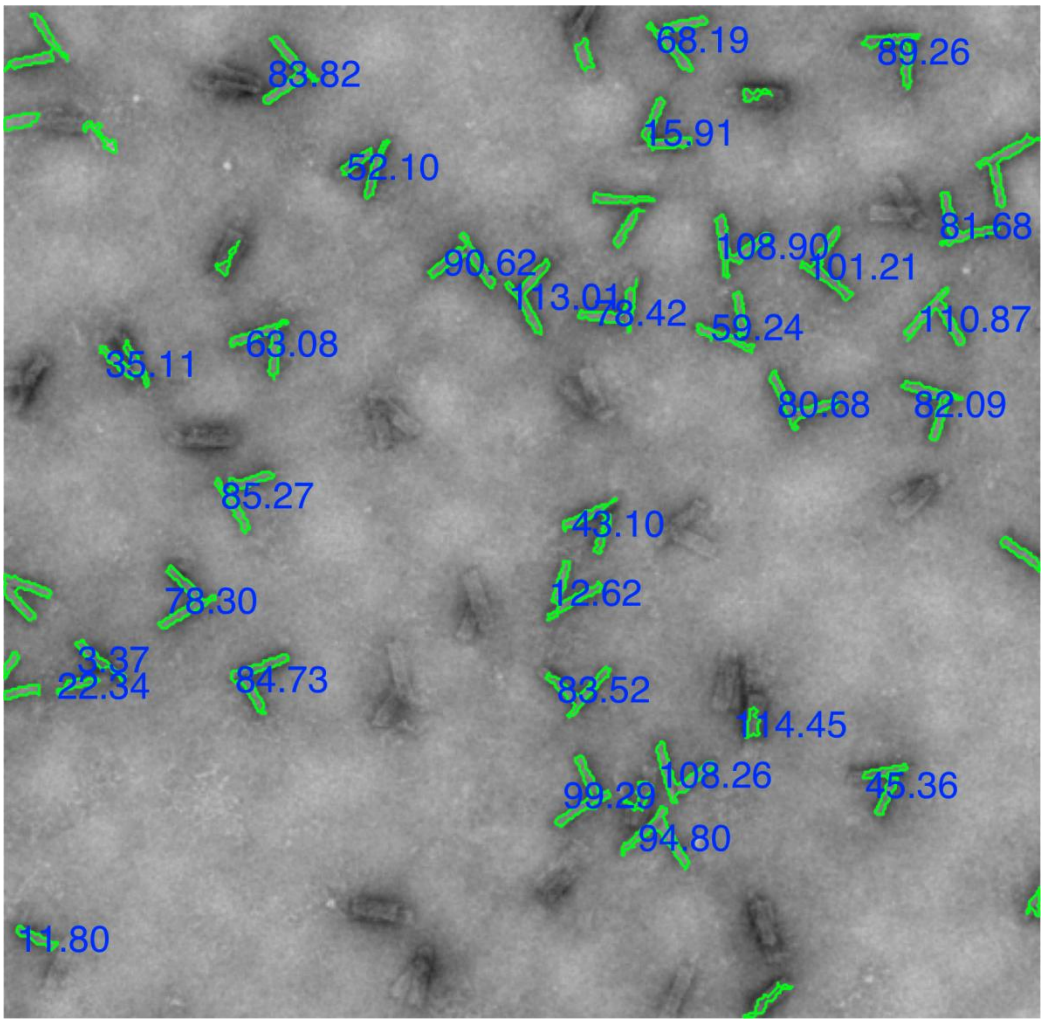

Figure 22: Nanocalipers analyzed with automated image processing software. Structures outlined in green have the angle between them calculated in blue.

Attempts have been made to apply this automated image processing to the filaments analyzed in this experiment. However, the unknown length and deflection of the filaments have presented a formidable barrier to moving beyond uniform geometry objects.

References

1. Castro, Carlos E. (2011, September). *Programming Biological Self-Assembly for the Design of Nanoscale Engineering Tools*. Powerpoint presented at the Institute of Materials Research Biomaterials Symposium, Columbus, OH.
2. Castro, Carlos E. et al. A primer to scaffolded DNA origami. *Nature Methods* **8**, 221-229 (2011).
3. Dietz, Hendrick. (2011, June). *Dietz Group Meeting*. Powerpoint presented at Technische Universität München Laboratory for Biomolecular Nanotechnology.
4. Douglas, SM., Chou, JJ., Shih, WM. "DNA-nanotube-induced alignment of membrane proteins for NMR structure determination", Proc Natl Acad Sci U.S.A., **104**, 6644-6648, (2007).
5. Douglas, Shawn M. et al. Self-assembly of DNA into nanoscale three-dimensional shapes. *Nature* **459**, 414–418 (2009).
6. Pastre et al., Biophys J, 85:2507 (2003).
7. Rothemund, Paul W.K. Folding DNA to create nanoscale shapes and patterns. *Nature* **440**, 297-302 (2006).

Appendix A: Sample CaDNAno Design

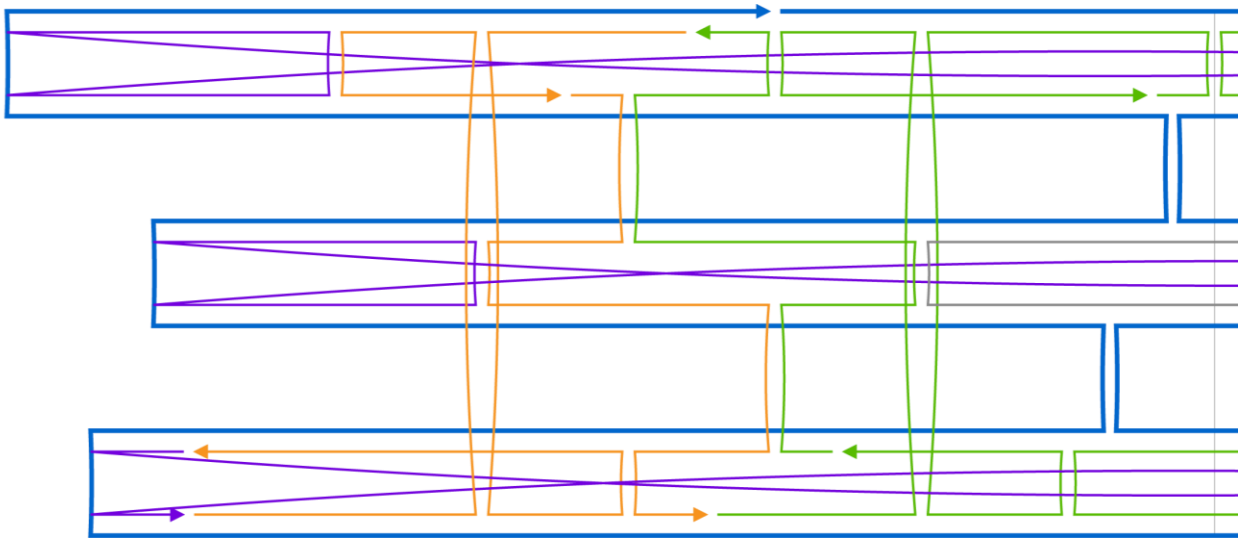

Figure 23: Left half of a sample 6 helix bundle CaDNAno design. Scaffold is blue, core staples are green, polymerization staples are purple, and orange staples separate the core and polymerization staples.

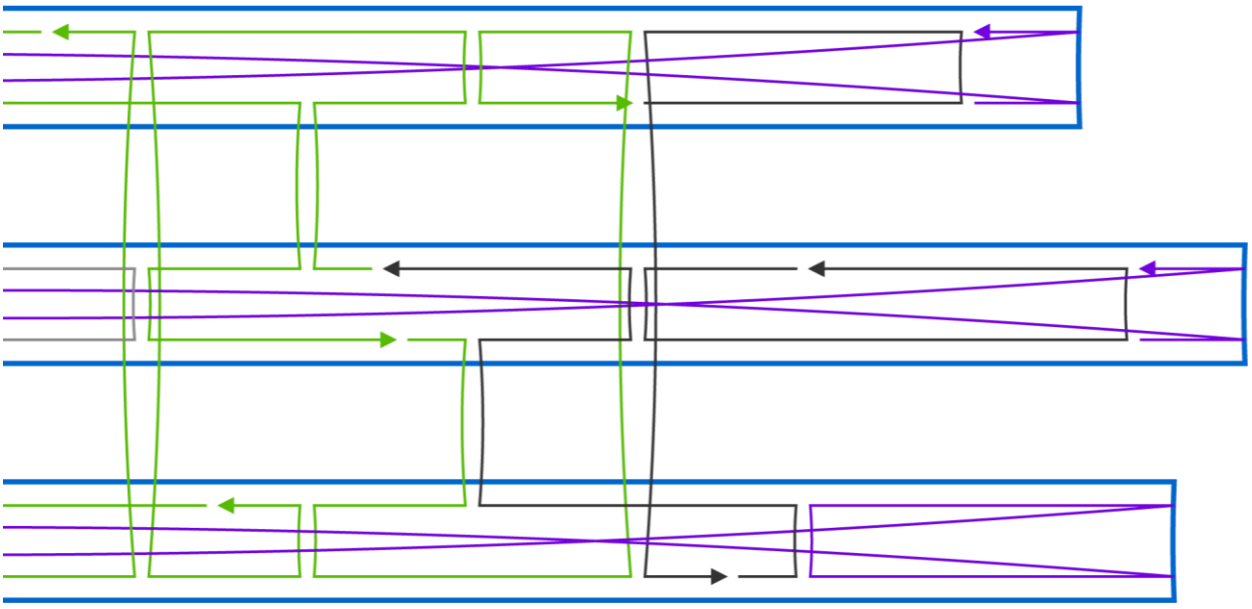

Figure 24: Right half of a sample 6 helix bundle CaDNAno design. Scaffold is blue, core staples are green, polymerization staples are purple, and black staples separate the core and polymerization staples.

Appendix B: Additional TEM Images

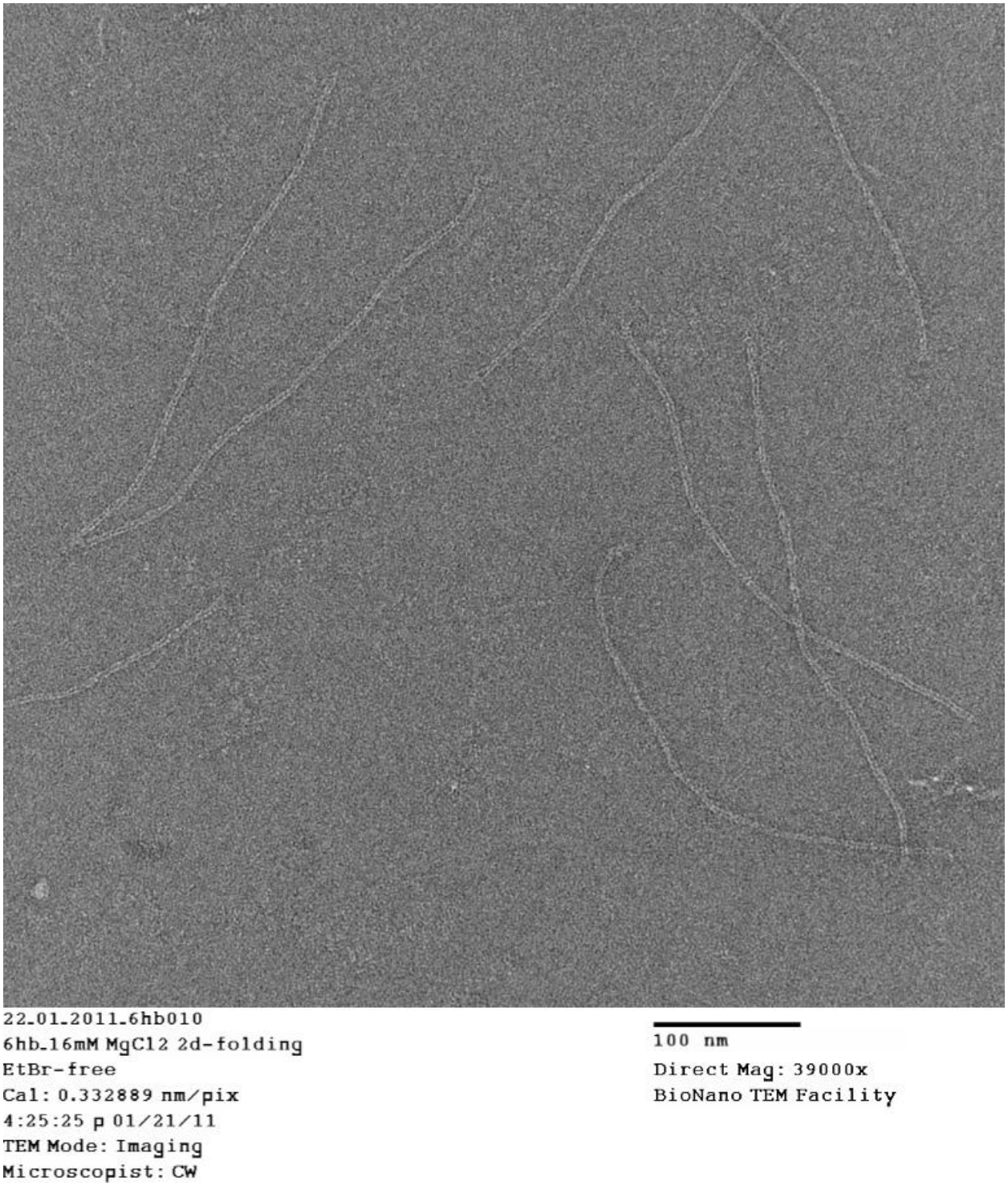

Figure 25: Additional image of the 6 helix bundle filaments.

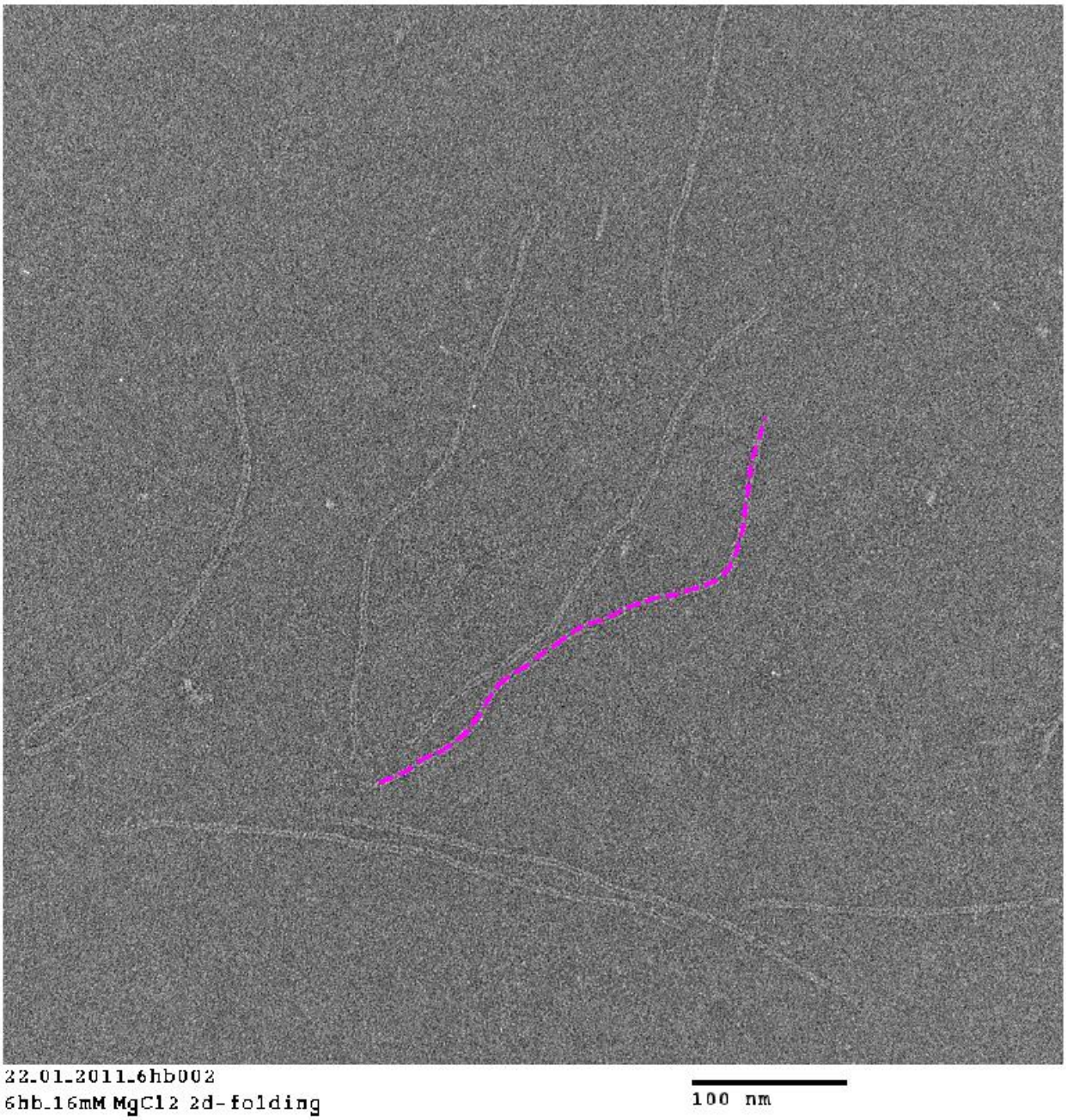

Figure 26: Additional image of the 6 helix bundle filaments.

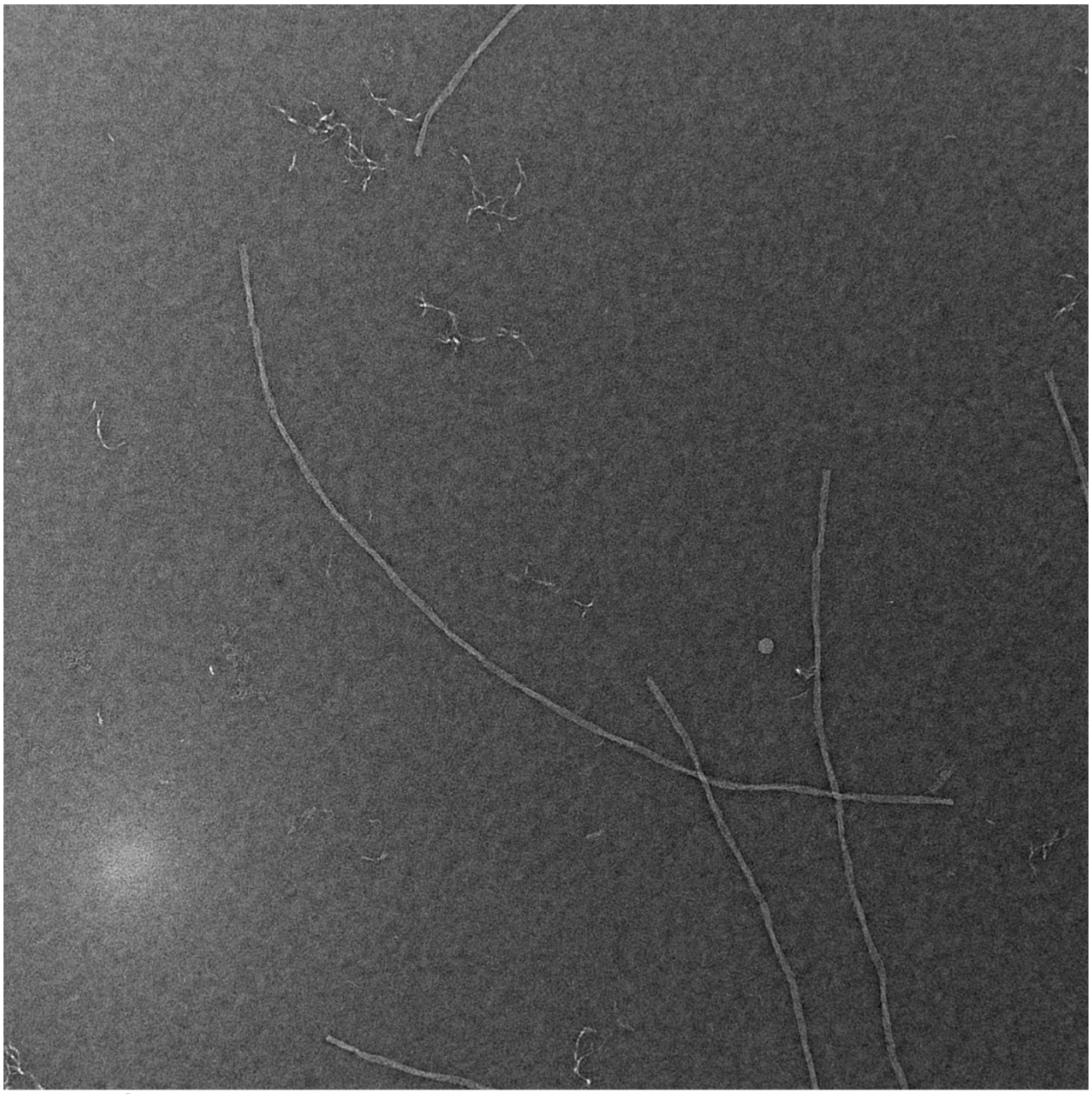

Figure 27: Additional image of the 18 helix bundle filaments.

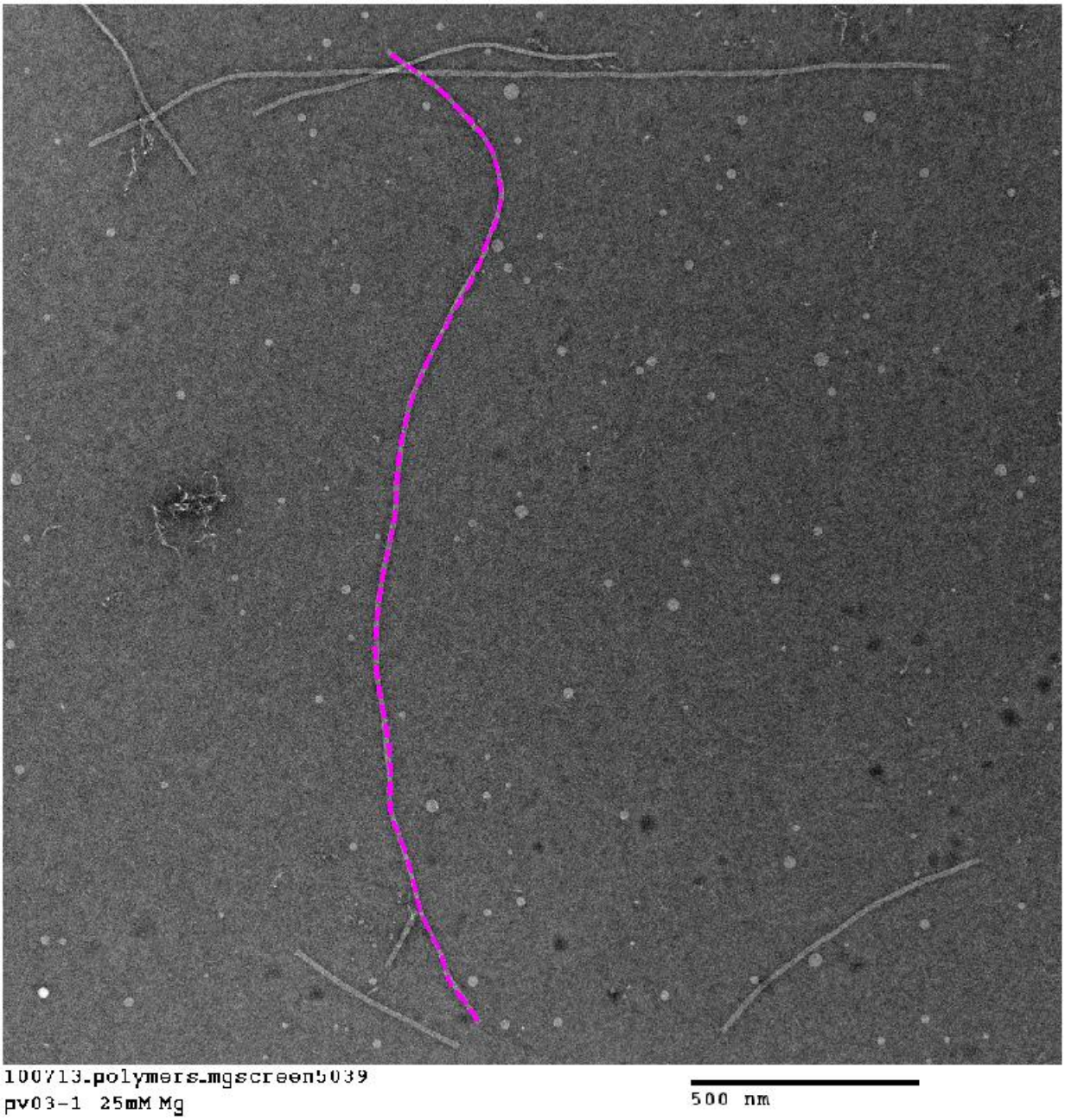

Figure 28: Additional image of the 18 helix bundle filaments.